Original Article

Enhanced interaction between genome-edited mesenchymal stem cells and platelets improves wound healing in mice

Journal of Tissue Engineering
Volume 15: 1–19

DOI: 10.1177/20417314241268917
journals.sagepub.com/home/tej
Sage

De-Yong Li[1,*], Yu-Meng Li[1,*], Dan-Yi Lv[1], Tian Deng[1], Xin Zeng[2], Lu You[1], Qiu-Yu Pang[1], Yi Li[3] and Bing-Mei Zhu[1]

Abstract

Impaired wound healing poses a significant burden on the healthcare system and patients. Stem cell therapy has demonstrated promising potential in the treatment of wounds. However, its clinical application is hindered by the low efficiency of cell homing. In this study, we successfully integrated P-selectin glycoprotein ligand-1 (*PSGL-1*) into the genome of human adipose-derived mesenchymal stem cells (ADSCs) using a Cas9-AAV6-based genome editing tool platform. Our findings revealed that *PSGL-1* knock-in enhanced the binding of ADSCs to platelets and their adhesion to the injured site. Moreover, the intravenous infusion of *PSGL-1-engineered* ADSCs (KI-ADSCs) significantly improved the homing efficiency and residence rate at the site of skin lesions in mice. Mechanistically, *PSGL-1* knock-in promotes the release of some therapeutic cytokines by activating the canonical WNT/β-catenin signaling pathway and accelerates the healing of wounds by promoting angiogenesis, re-epithelialization, and granulation tissue formation at the wound site. This study provides a novel strategy to simultaneously address the problem of poor migration and adhesion of mesenchymal stem cells (MSCs).

Keywords
Cas9-AAV6, PSGL-1, Platelets, WNT/β-catenin, MSC homing

Date received: 20 March 2024; accepted: 26 June 2024

Introduction

The skin, as the body's largest defensive organ[1], is susceptible to a various external stimuli such as solid impacts, violent friction, and sharp cuts, leading to skin trauma.[2,3] While minor skin injuries can heal naturally, severe wounds, especially chronic wounds, often fail to heal effectively without appropriate treatment due to microbial invasion and accumulated inflammation.[4,5] The annual cost of wound treatment and care is estimated to be in the tens of billions of dollars, creating a significant burden on both patients and medical systems.[6] Additionally, nonhealing wounds can result in life-threatening conditions like amputation and serious illness. Therefore, it is crucial to promptly close post-wound sites to prevent infection, inhibit scar formation, and promote healing. Stem cell therapy has emerged as a promising approach for wound treatment[7,8], as stem cells can migrate, adhere to the wound site, and release cytokines and growth factors which can activate intrinsic cells to initiate the regeneration process.

[1]Regenerative Medicine Research Center, West China Hospital, Sichuan University, Chengdu, Sichuan, China
[2]Key Laboratory of Transplant Engineering and Immunology, National Clinical Research Center for Geriatrics, Frontiers Science Center for Disease-related Molecular Network, West China Hospital, Sichuan University, Chengdu, China
[3]Core Facilities of West China Hospital, Sichuan University, Chengdu, China

*These authors contributed equally to this work and should be considered co-first authors.

Corresponding author:
Bing-Mei Zhu, Regenerative Medicine Research Center, West China Hospital, Sichuan University, No. 1 Keyuan 4th Road, Gaopeng Ave, Chengdu, Sichuan 610041, China.
Email: zhubm@wchscu.cn

They act as a "repository" of regenerative molecules.[9] To achieve successful clinical application of MSCs, it is essential to ensure effective migration and adhesion of transplanted cells to damaged tissues following administration. However, the therapeutic efficacy of stem-cell therapy is limited by poor homing efficiency, with only a small percentage of the infused cells reaching the injured site.[10] Homing involves a complex interplay of factors such as chemokines, growth factors, and adhesion molecules, working together to facilitate the migration of stem cells.[11] Some studies have explored modifying chemokine receptors to enhance the therapeutic efficacy of infused MSCs by improving homing.[12–15] Nevertheless, the high shear stress in the blood flow can disrupt the chemokine gradient at the injury site, hindering MSCs' effective adherence to the injured tissue.[16] Also, some studies have focused on increasing the expression of adhesion molecules to improve the attachment of locally transplanted MSCs[17–19]. However, it is important to note that orthotopic transplantation has limited applicability to specific and accessible drug administration sites.[20] Therefore, the development of a novel strategy is necessary to simultaneously enhance MSCs' migration and adhesion to injured tissues, ultimately improving their therapeutic effect on chronic wound healing.

Platelets are a type of anucleated cells that contain various receptors in the membrane, including integrin, selectin, lipids, and immunoglobulin superfamily.[21] In case of skin injury, platelets rapidly aggregate to form thrombosis and recruit immune cells for wound healing.[22] Therefore, besides their role in hemostasis, platelets possess the natural ability to target the injured site.[23,24] Cellular adhesion is mediated by four major classes of adhesion molecules: cadherins, integrins, immunoglobulin superfamilies, and selectins. Furthermore, cell adhesion molecules (CAM) play an essential role in various physiological and pathological conditions.[25–27] Targeting the highly expressed adhesion molecules at the wound site, selecting specific and relevant adhesion molecule ligands to promote the conjugation of MSCs to platelets and adhesion to the injury site without interfering with other normal cell functions is one of the optimal schemes to improve the homing efficiency and therapeutic effect of MSCs.

Here, we demonstrated that the expression of selectin family members (SELL, SELP) rapidly increased within 24 h after mouse skin injury, while SELP was also expressed on the membrane of activated platelets. ADSCs did not express PSGL-1, a high-affinity ligand for selectin. Knock-in of *PSGL-1* in ADSCs promoted platelets binding and adhesion to injured endothelial cells, altered proliferation, migration, anti-apoptosis, and paracrine abilities of these cells in vitro. Besides, the homing efficiency of these cells to injured tissues was enhanced by intravenous infusion in a mouse model of skin wounds with total corticectomy. Mechanistically, *PSGL-1* knock-in significantly increased the formation of PSGL-1/β-catenin protein complex and the level of activated β-catenin protein in the nucleus. Knock-down of β-catenin by siRNA abolished *PSGL-1* knock-in induced improved phenotypes, including proliferation and paracrine.

Materials and methods

Animals

Our study adhered to the ARRIVE guidelines for the reporting of animal experiments, and all animal procedures were approved by the Animal Care Committee at Sichuan University West China Hospital (No.20220318012), following the Guidelines for the Care. Male C57BL/6 mice were procured from GemPharmatech Co. Ltd. in Chengdu, China, and were raised in a specific pathogen-free laboratory animal facility at West China Hospital. The mice were kept on a 12-hour light-dark cycle with ad libitum access to food and water. Cutaneous wound healing models were established using eight-week-old male C57 mice. Euthanasia was conducted by cardiac puncture under isoflurane anesthesia, and any mice that expired before the planned euthanasia times were excluded from the study. Each experimental unit consisted of a single animal, and the control groups included PBS-treated and CON-ADSCs-treated animals.

Isolation of ADSCs

Adipose tissues were obtained from healthy person through liposuction, which was approved by the Biomedical Ethics Review Committee of West China Hospital of Sichuan University (No. 2022-267). ADSCs were obtained from human adipose tissue. The tissue was finely chopped and treated with 0.1% collagenase type I (Gibco Life Technologies, New York, NY, USA) for 2–3 h at 37°C. After stopping the digestion process with Minimum Essential Medium-α (α-MEM) supplemented with a 5% Serum substitute (Helios Bioscience, HPCFDCRL50, Atlanta, GA, USA), the solution was filtered through a 100-μm filter and centrifuged at 1400 rpm for 5 min. The remaining deposit was washed twice with α-MEM and then resuspended and cultivated in a T75 flask.

Ex vivo genome editing of ADSCs

Cells were cultured in Opti-MEM I medium (Invitrogen, 11058021, New York, NY, USA) at a concentration of 5000 cells per microliter (μL). To create a pre-complexed RNP, nucleases, and sgRNA were combined with a molar ratio of 2.5:1 (sgRNA-to-Cas9) and a final concentration of 0.3 μg/μL Cas9 protein (Integrated DNA Technologies, 1081059, Coralville, IA, USA). The MSC-Nuclease mixtures were electroporated using pulse code CM-119 on the Lonza 4D Nucleofector (Lonza, Basel, Switzerland). Immediately after electroporation, the mixtures were diluted with a 2× volume of Opti-MEM I. In cases where

a repair template was required, adeno-associated virus 6 (AAV6) vector genomes were added to the mixture at a concentration of $1.0*10^5$ vector genomes/cell. The MSC-AAV6 mixtures were then incubated at 37°C for 15 min before being seeded at a density of approximately 220 cells/cm^2 in a complete culture medium. The medium was replaced 48 h after infection to ensure optimal conditions for further experiments.

Flow cytometry and FACS

The efficiency of integrating the fluorescence gene was assessed using flow cytometry at various time points after targeting. To ensure purity, the $EGFP^{+high}$ or $EGFP^{-}$ populations obtained at one passage post-targeting were sorted using a BD FACS II Aria SORP (BD Biosciences, San Jose, CA, USA) and subsequently expanded for additional analyses and application in animal models.

Phenotypic analysis by flow cytometry

After two washes with PBS, the cells were resuspended and incubated for 15 min at room temperature with pre-labeled antibodies. The cells were then washed twice more with PBS and resuspended in 300 µL of PBS. Flow cytometry analysis was performed using a Beckman Coulter Life Sciences instrument located in Indianapolis, IN, USA. The obtained data were analyzed using Cytexpert and Flow Jo software to generate histograms.

Cell differentiation capacity analysis

To assess adipogenic differentiation ability, $5*10^4$ cells were seeded in six-well plates. After reaching full confluence, cells were treated with ADBM-A (Cyagen, Santa Clara, CA, USA) for 3 days, followed by ADBM-B (Cyagen, Santa Clara, CA, USA) for 1 day. The alternating between ADBM-A and ADBM-B was repeated for 3–5 cycles. The lipid droplets were visualized by staining with fresh Oil Red-O (Sigma-Aldrich, 1320-06-5, New Brunswick, NJ, USA) solution and subsequently photographed.

To evaluate the osteogenic differentiation capacity, $5*10^4$ cells were plated in six-well plates until they reached 70% confluence. The cells were then cultured in osteogenic differentiation basal medium (ODBM, Cyagen, Santa Clara, CA, USA) for a duration of 3 weeks. Following this, they were fixed in 4% paraformaldehyde and stained with Alizarin Red.

For the investigation of chondrogenic differentiation capacity, a total of $5*10^5$ cells were centrifuged and collected at the bottom of a 15 mL centrifuge tube. Subsequently, the culture medium was replaced with chondrogenic differentiation basal medium (CDBM, Cyagen, Santa Clara, CA, USA) for 4 weeks after the cells were condensed into pellets. The capacity of ADSC pellets to differentiate towards chondrocyte pellets was evaluated using Alcian blue staining.

Real time quantitative reverse transcription polymerase chain reaction (RT-qPCR)

RNA was isolated from CON-ADSCs and KI-ADSCs using TRIZOL reagent (Invitrogen™, 15596026, New York, NY, USA). Subsequently, 1.0 µg of total RNA was subjected to reverse transcription into cDNA utilizing Hiscript III Reverse Transcriptase (Vazyme, R302, Nanjing, China). qPCR analysis was performed using Hieff® qPCR SYBR Green Master Mix (Yeasen, 11201ES50, Shanghai, China) and an ABI 7900HT fast real-time PCR system (Applied Biosystems, QuantStudio 6 Flex, Ajo, AZ, USA). Triplet measurements were taken for each sample. Comprehensive information regarding primer sequences can be found in Supplemental Table 1, encompassing the transcription levels of fibroblast growth factor (b-FGF), angiopoietin1 (ANG1), collagentypeIalpha1 (COL1a1), hepatocyte growth factor (HGF), chemokine (C-X-C Motif) ligand 12 (CXCL-12), collagentypeIalpha3 (COL3a1), insulin-like growth factor (IGF), and vascular endothelial growth factor A (VEGFA). All genes were normalized to the endogenous reference gene ACTB. The mRNA expression levels of the target genes were determined using the DDCt method.

Conditioned medium of ADSCs

CON-ADSCs and KI-ADSCs were cultured until 70%–80% confluence, washed with PBS, and incubated for 48 h in α-MEM to obtain conditioned medium. The medium was then centrifuged at 3000 rpm for 5 min at 4°C and stored at −80°C.

Elisa analysis

The conditioned medium (CM) of ADSCs was obtained using the method described earlier. To assess the levels of HGF, VEGFA, and IGF in the CM, an enzyme-linked immunosorbent assay (ELISA) was conducted. The ELISA assay kits used for HGF (Elabscience, ER242RB), VEGFA (Elabscience, E–EL–H0111c), and IGF (Elabscience, E–EL–H0086c) were employed, following the instructions provided by the manufacturer.

Western blotting analysis

Skin tissues and cell suspension were lysed in RIPA lysis buffer (MB–030–0050, Multi Sciences Biotech, Hangzhou, China) supplemented with phenylmethylsulfonyl fluoride. Protein concentrations were determined using a BCA Protein Assay Kit (23225, Thermo Fisher, Waltham, MA, USA). Total proteins of equal quantity were then separated on 4%–20% SDS–PAGE gel (ACE Biotechnology, Nanjing, China), and transferred onto PVDF membranes (Millipore, NJ, USA). After blocking with 5% skimmed milk and washing with tris–buffered saline containing 0.1% tween–20 (TBST), the protein

bands were incubated with primary antibodies (Supplemental Table 2 for antibody information) overnight at 4°C. Post washing with TBST, the protein bands were probed with HRP-conjugated secondary antibody and visualized using ECL buffer (32,209, Thermo Fisher, Waltham, MA, USA). The western blotting results were quantified using ImageJ.

Establishment of a cutaneous wound healing model

To establish cutaneous wound healing models, we used 8-week-old male C57 mice. Anesthesia was induced by administering pentobarbital sodium (i.p. injection, 50 mg/kg), and a full-thickness skin injury with a diameter of 4 mm was created on the dorsal region of each mouse. To prevent contracture, hydrogel was applied to the wounds. Subsequently, the mice were randomly assigned to one of three groups: CON-ADSCs group ($n=20$), KI-ADSCs group ($n=23$) with 1*106 cells in 100 µL PBS, or 100 µL PBS group ($n=16$). Mice were housed separately. The wounds were photographed on days 0, 3, and 7 to monitor the healing progress. The wound healing rate was calculated using the following formula: Dn wound healing rate = (D0 wound area − Dn wound area)/D0 wound area × 100%.

IVIS observation

CON-ADSCs group ($n=6$) and KI-ADSCs group ($n=7$) marked with DiR were transplanted into mice via tail vein injection at a dosage of $1*10^6$ cells per mouse. DiR imaging was performed with an excitation/emission of 710/760 nm, high lamp level, medium binning, filter 1, and 1.0 s exposure time. Living Image software version 4.3 (Xenogen) was used to analyze the grayscale and fluorescent images of each sample, with regions of interest automatically drawn over the signals and manual corrections made based on the grayscale image. Quantification of DiR-labeled cell distribution in each organ was performed using Cho et al.'s[19] method with some modifications, with the average radiant efficiency of the organs to the background calculated to reduce variability.

Histological observation

The tissue samples taken on day 3 and day 7 after the wound were treated with 4% paraformaldehyde at 4°C overnight. Then, the samples underwent dehydration using graded ethanol concentrations (30%, 50%, 70%, 80%, 90%, and 100%), xylene, and paraffin washes. Thick sections measuring approximately 4–6 mm were prepared from the paraffin-embedded wound tissues and subjected to staining using Masson's trichrome. The stained tissue sections were examined using a microscope.

Targeted binding of KI-ADSCs to activated HUVECs and platelets

HUVECs were purchased from American Type Culture Collection (ATCC, USA). HUVECs were cultured in tissue-culture-treated 6-well plates until they reached confluence. Before the experiment, the HUVECs were treated with 10 ng/ml of tumor necrosis factor-α (TNF-α) for 6 h. After washing the cells with fresh ECM culture medium, a suspension of CON-ADSCs or KI-ADSCs ($5*10^4$ cells/mL) was added to each well and incubated at 37°C with shaking. After an hour, the unbound cells were removed by rinsing with PBS. The specific binding of KI-ADSCs to activated HUVECs was observed using confocal microscopy.

Statistical analysis

The data obtained from the mouse and cell model were presented as the mean ± standard deviation (SD). To determine significant differences, a two-tailed independent-sample *t*-test was utilized for comparing two groups, while a one-way analysis of variance (ANOVA) followed by a Tukey post hoc test was employed for comparing multiple groups. A *p*-value less than 0.05 was considered to indicate statistical significance. All the statistical analyses were conducted using GraphPad Prism software.

Results

PSGL-1 *is a potential target for improving MSCs homing*

To investigate the changes in cell-cell adhesion molecules following injury, we conducted an analysis of multiple transcriptomes from different studies (Supplemental Table 3). Given the expeditious targeting of the injured site facilitated by the exogenous infusion of stem cells,[28] our study focused primarily on genes that showed enrichment during the early stages of damage (Figure 1(a)). Notably, there were significant alterations observed in the L-selectin (*Sell*) and P-selectin (*Selp*) during the early stage of wound healing (Figure 1(b)).

Platelets possess a natural targeting ability to localize at sites of injury, inflammation, and tumors, allowing them to accumulate rapidly at the injured site and mediate the recruitment of immune cells, thereby facilitating early-stage wound healing. It is important to note that SELP is expressed on the membrane of platelets. PSGL-1, a high-affinity ligand for the selectin family, has been reported to serve as a ligand for both SELL and SELP.[29] It plays a critical role in the initial adhesion phase of leukocyte migration across the endothelium. However, ADSCs do not express PSGL-1.[30] Therefore, surface modification of ADSCs to express PSGL-1 may enhance their interaction with platelets and promote adhesion to the injured site, thereby improving their homing efficiency.

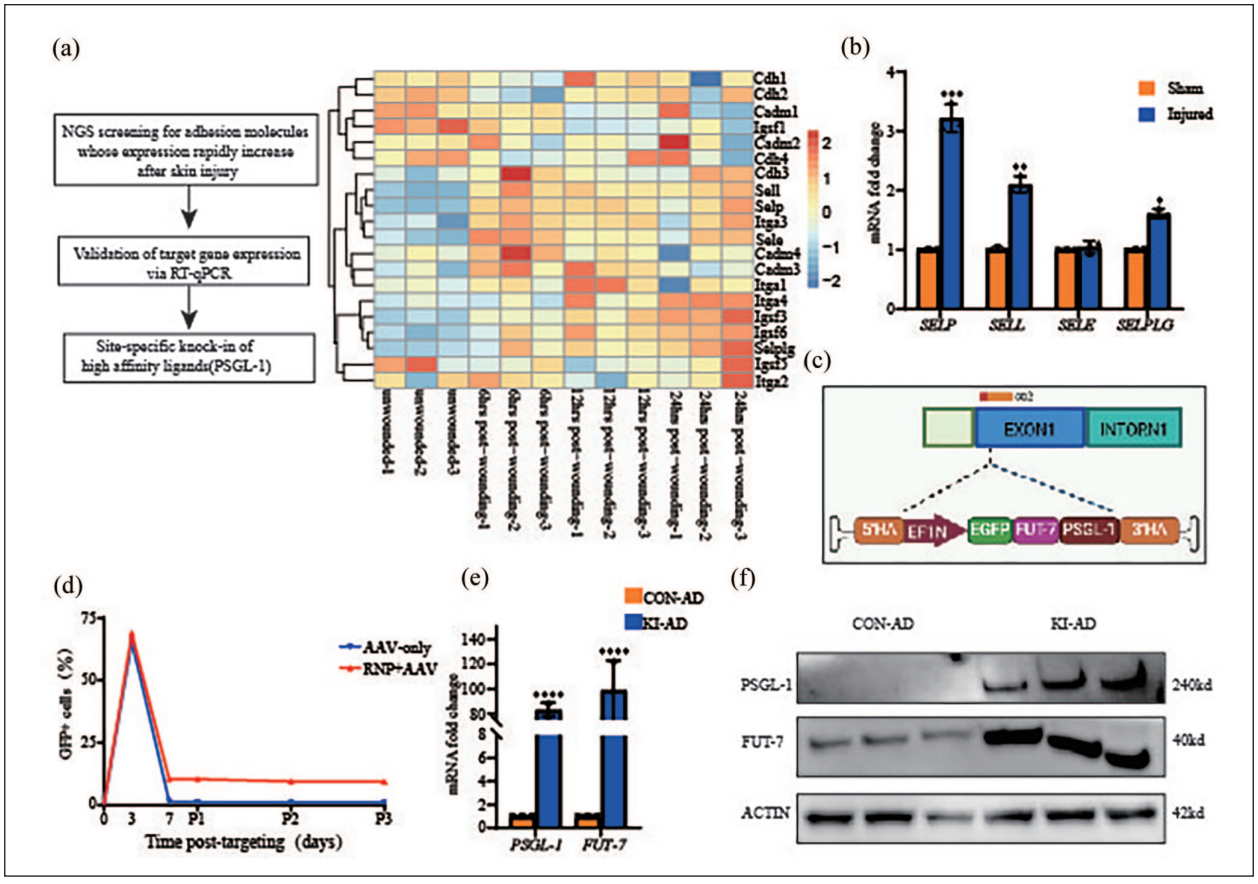

Figure 1. The screening process for target genes and the corresponding sgRNA. (a) Schematic depiction of the overall workflow. The expression levels of adhesion molecules were evaluated at 6h, 12h, and 24h after induction of skin injury. (b) RT-qPCR analysis of *SELP*, *SELL*, *SELE*, and *SELPLG* expression 24 hours after skin injury modeling ($n = 3$). (c) Design of the rAAV6-PSGL-1 donor. (d) Flow cytometry analysis of the average frequency of EGFP$^+$ cells in ADSCs was evaluated at multiple time points following co-incubation ($n = 3$). In the control group, cells were not subjected to RNP addition during electroporation, precluding homologous recombination events. Consequently, the proportion of EGFP$^+$ cells exhibited a decline concomitant with cell proliferation. (e) RT-qPCR analysis of PSGL-1 and FUT-7 expression in CON-ADSCs and KI-ADSCs ($n = 3$). This and subsequent experiments exclusively employed CON-ADSCs, obtained through flow cytometry sorting, which ensured sustained expression of EGFP via homologous recombination. (f) Western blotting analysis of expression PSGL-1 and FUT-7 in CON-ADSCs and KI-ADSCs ($n = 3$). Data are shown as mean ± SD. Independent-sample *t*-test (two-tailed) was used for statistical comparisons between two groups. $^*p < 0.05$, $^{**}p < 0.01$, $^{***}p < 0.001$, $^{****}p < 0.0001$.

Furthermore, it is worth mentioning that the effective interaction between PSGL-1 and selectin receptors requires glycosylation of PSGL-1 by the enzyme Fucosyltransferase 7 (FUT-7).[29,31] In this study, we employed a CRISPR/Cas9-based approach to achieve precise site-specific integration in ADSCs, resulting in stable expression of both *PSGL-1* and *FUT-7*. This modification potentially improves the adhesive properties of ADSCs and their homing ability to injured sites.

Cas9-AAV6 mediated Knock-in ensured a successful targeted integration of PSGL-1 *in ADSCs*

Efficient delivery of the Cas9-AAV6 tool has been previously shown to be critical for successful gene knock-in.[32–35] To accomplish transgenic integration in ADSCs, we utilized electroporation to deliver CRISPR/Cas9 system while AAV6 was used to deliver homologous repair templates. To begin, we designed 10 sgRNAs targeting different exons of the *HBB* gene locus using an online platform (Supplemental Figure 1A, Supplemental Table 4). Among these sgRNAs, sgRNA2 exhibited exceptional efficiency, with a cleavage efficiency exceeding 95% in ADSCs (Supplemental Figure 1B and C). To enable efficient homology-directed repair (HDR), a recombinant adeno-associated virus 6 (rAAV6) vector was constructed as the donor template. This rAAV6-PSGL1 donor template incorporated essential components such as a EGFP expression cassette, homology arms centered around the break site, and cDNA of *PSGL1* and *FUT7* (Figure 1(c), Supplemental Table 5). Following the construction of the rAAV6-PSGL1 donor template, the subsequent step involved determining the optimal concentration of the AAV6 virus vector to ensure efficient infection. Our results

indicated that the most favorable electroporation-assisted transduction (EAT) occurred at an incubation rate of $1*10^5$ vector genomes per cell (Supplemental Figuer 2A), with no alterations in cell viability observed after 2 days of infection at this concentration (Supplemental Figure 2B and C). With these detailed confirmations, subsequent gene knock-in experiments at the *HBB* locus were conducted (Supplemental Figure 3A).

When utilizing sgRNA, Cas9, and AAV6 repair templates, the frequency of $EGFP^+$ ADSCs reached its peak 3 days after targeting and remained stable from days 3 to 7. To further analyze the integration efficiency, Fluorescence Activated Cell Sorting (FACS) was performed 7–10 days after AAV6 treatment. The results revealed that the percentage of targeted integration in ADSCs was $10\% \pm 2\%$, and the EGFP signal persisted for at least three passages (Figure 1(d), Supplemental Figure 3B). Notably, when using only the AAV6 vector, the $EGFP^+$ population was observed initially, but this population significantly diminished after one passage in culture (Supplemental Figure 3C). The presence and subsequent disappearance of the $EGFP^+$ population in *AAV6*-treated cells align with the gene expression dynamics of AAV fragments diluted by cell proliferation. These rapid clearance kinetics after AAV-only delivery and transient EGFP expression highlight the limitations of relying solely on exogenous expression to enhance MSC efficacy. To further validate the targeted knock-in of *PSGL-1* and *FUT-7*, genomic DNA was extracted from the cells for PCR followed by agarose gel electrophoresis and sequencing. Both methods confirmed the successful integration of the recombinant fragments (Supplemental Figure 4). Moreover, RT-qPCR and western blotting results demonstrated the transcription and translation of these two genes, *PSGL-1* and *FUT-7*, in ADSCs (Figure 1(e) and (f)).

In addition, we evaluated the maintenance of stemness in knock-in cells according to the standard definition of mesenchymal stem cells established by the International Association for Cell Therapy.[36] Specifically, we examined the expression of specific surface markers and the capacity for three-dimensional differentiation into adipocytes, osteoblasts, and chondrocytes. Notably, the results revealed that gene knock-in did not affect the expression of surface markers associated with mesenchymal stem cells nor their ability for three-dimensional differentiation (Supplementl Figure 5). In summary, we successfully generated knock-in ADSCs for *PSGL-1* and *FUT-7* using the Cas9-AAV6 platform, while preserving the ex vivo properties of ADSCs in terms of their stemness and differentiation potential.

The knock-in of PSGL-1 *promoted ADSCs binding to platelets and adhesion to activated human umbilical vein endothelial cells (HUVECs)*

The knock-in of *PSGL-1* in ADSCs holds the potential for enhanced platelet capture and targeted adhesion at the wound site through SELP-PSGL-1 interaction. To assess this capability, DiO-labeled KI-ADSCs or CON-ADSCs were co-incubated with Dil-labeled platelets. Fluorescence imaging demonstrated efficient binding of KI-ADSCs (green) to platelets (red), while CON-ADSCs showed limited binding (Figure 2(a)). Furthermore, flow cytometry analysis revealed that, following an hour of co-incubation, 55% of KI-ADSCs formed aggregates with platelets (Figure 2(b) and (c)). Subsequently, we investigated whether this increased binding capacity would lead to excessive platelet aggregation and thrombosis, a potential risk during cell administration. The results showed that the increased binding efficiency of ADSCs to platelets didn't significantly promote platelet aggregation or thrombus formation (Figure 2(d)–(f)).

Furthermore, we simulated changes in the adhesion of ADSCs to injured tissue by adhesion to endothelial cells in vitro. Tumor necrosis factor-α (TNF-α) preconditioning was employed to activate HUVECs and then the adhesion of ADSCs to HUVECs was assessed (Supplemental Figure 6). Immunofluorescence staining revealed that the adhesion to HUVECs didn't significantly change without TNF-α pretreatment between KI-ADSCs and CON-ADSCs (Supplemental Figure 7). However, when HUVECs were pretreated with TNF-α, the adhesion of KI-ADSCs to HUVECs was significantly increased. Platelet-rich plasma (PRP) contains various growth factors and cytokines that can modulate cellular interactions. Moreover, to explore the potential impact of PRP on the adhesion of KI-ADSCs to activated HUVECs, we conducted additional experiments. The results demonstrated that binding platelets with KI-ADSCs significantly enhances the adhesion of ADSCs to activated HUVECs (Figure 2(g) and (h)). These findings suggested that KI-ADSCs possessed excellent binding ability to both activated HUVECs and platelets.

KI-ADSCs showed better retention at the wound site in mice

A skin injury model was established by a 4mm full-thickness punch biopsy on the backs of 10-week-old c57 mice. To prevent wound contraction, the wounds were fixed using hydrogel. Subsequently, $1*10^6$ KI-ADSCs or CON-ADSCs were promptly administered via tail vein infusion to assess disparities in cellular homing (Figure 3(a)). After 24 h post-cell administration, fluorescent imaging revealed a markedly increased fluorescence signal surrounding the wounds in the KI-ADSCs treatment group compared to the CON-ADSCs treatment group (Figure 3(b) and (c)). Immunostaining analyses revealed the accumulation of a significantly greater number of infused MSCs (EGFP-labelled cells) in the injured sites of the KI-ADSCs-infused group than in the CON-ADSCs-infused group on Day1 (Figure 3(d) and (e)). Besides, ex vivo organ imaging demonstrated a substantial decrease in fluorescence signal intensity within non-target organs in

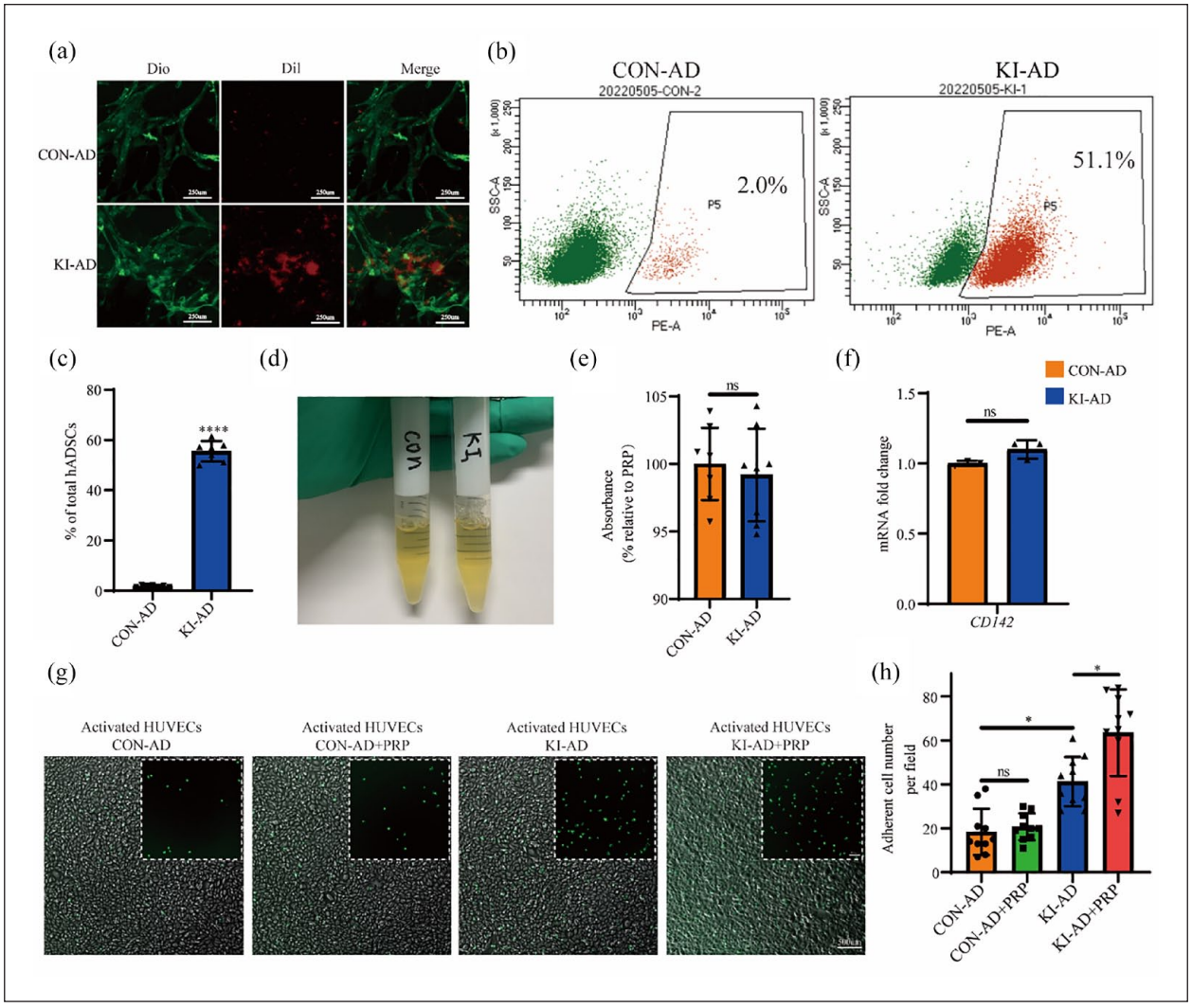

Figure 2. *PSGL-1*-engineered ADSCs exhibited enhanced binding and adhesion capabilities to platelets and HUVECs. (a) Fluorescence microscopy was employed to assess the binding ability of CON-ADSCs and KI-ADSCs to platelets. DIO-labeled ADSC and Dil-labeled platelets ($n = 3$). ADSCs co-incubated with platelets for 1 hour. Scale bars, 200 μm. (b, c) Flow cytometry analysis of the binging ability of ADSCs to platelets ($n = 6$). (d, e) Absorbance analysis of platelet aggregation induced by the addition of ADSCs ($n = 6$). (f) RT-qPCR analysis of tissue factor CD142 in ADSCs to gauge its ability to promote thrombosis ($n = 3$). (g, h) Fluorescence microscopy analysis of the binding number of CON-ADSCs, CON-ADSCs+PRP, KI-ADSCs, and KI-ADSCs+PRP co-cultured with activated HUVECs after 1h. ($n = 10$). Scale bars, 500 μm. Data are shown as mean ± SD. Independent-sample *t*-test (two-tailed) was used for statistical comparisons between two groups; One–way ANOVA followed by Tukey post hoc test was used for statistical comparisons between multiple groups.
*$p < 0.05$, ****$p < 0.0001$.

the KI-ADSCs treatment group compared to the CON-ADSCs treatment group (Figure 3(f) and (g)). As time progressed, the transplanted cells gradually diminished and died. Extensive cell loss was observed on days 3 and 7 after cell administration via in vivo fluorescent imaging, which was significantly reduced in the KI-ADSCs treatment group compared to the CON-ADSCs treatment group (Figure 3(h)). Notably, the analysis of $CD4^+$ T cells and $CD8^+$ T cells within peripheral blood $CD3^+$ lymphocytes (Supplementary Fig8A), as well as the histopathological examination of the spleen (Supplementary Fig8B), suggested that systemic administration of ADSCs did not induce immunogenicity. Furthermore, the long-term distribution of ADSCs within non-target organs, including the liver, lung, and kidney, did not result in any discernible organ damage (Supplemental Figure 8C). These findings

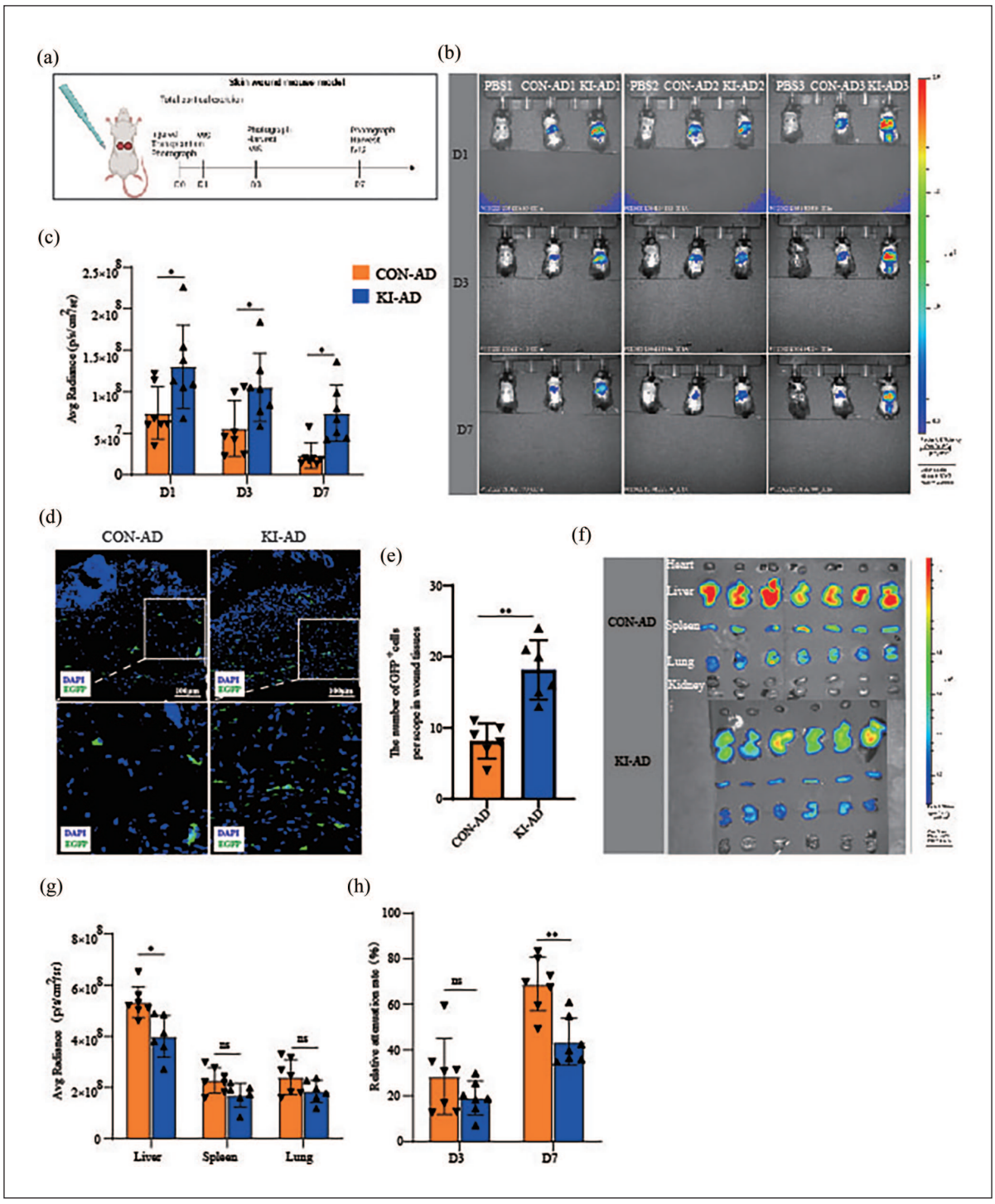

Figure 3. *PSGL-1*-engineered ADSCs exhibited enhanced homing efficiency and retention to mouse wound tissue. (a) Schematic representation of animal experiments. The animal experiments entailed the application of hydrogel to wounds for the purpose of moisturization and prevention of wound contraction. The wound area was measured relative to the constant size of the silicone ring and then normalized to the initial wound area (day 0). (b) *in vivo* fluorescence imaging of mice. Mice were anesthetized by isoflurane, and the wound was observed at D1, D3, and D7 after intravenous injection of PBS, DiR-labeled CON-ADSCs, or KI-ADSCs ($n = 7$). (c) Quantification analysis of the fluorescence intensity in wounds. (d) Immunostaining analysis of $EGFP^+$ cells accumulated in the wound tissues from the CON-ADSCs-infused group and KI-ADSCs-infused group in 1 day. (e) Quantitative analysis of cell engraftment by histology ($n = 6$). (f) *Ex vivo* fluorescence imaging of heart, liver, spleen, lung, and kidney ($n = 6$). (g) Quantification analysis of the fluorescence intensity in various organs one day after cell transplantation. (h) The relative fluorescence attenuation rate of D3 and D7 compared to D0 within the same mouse. Data are shown as mean ± SD. Independent-sample t-test (two-tailed) was used for statistical comparisons between two groups.
$^*p < 0.05$, $^{**}p < 0.001$.

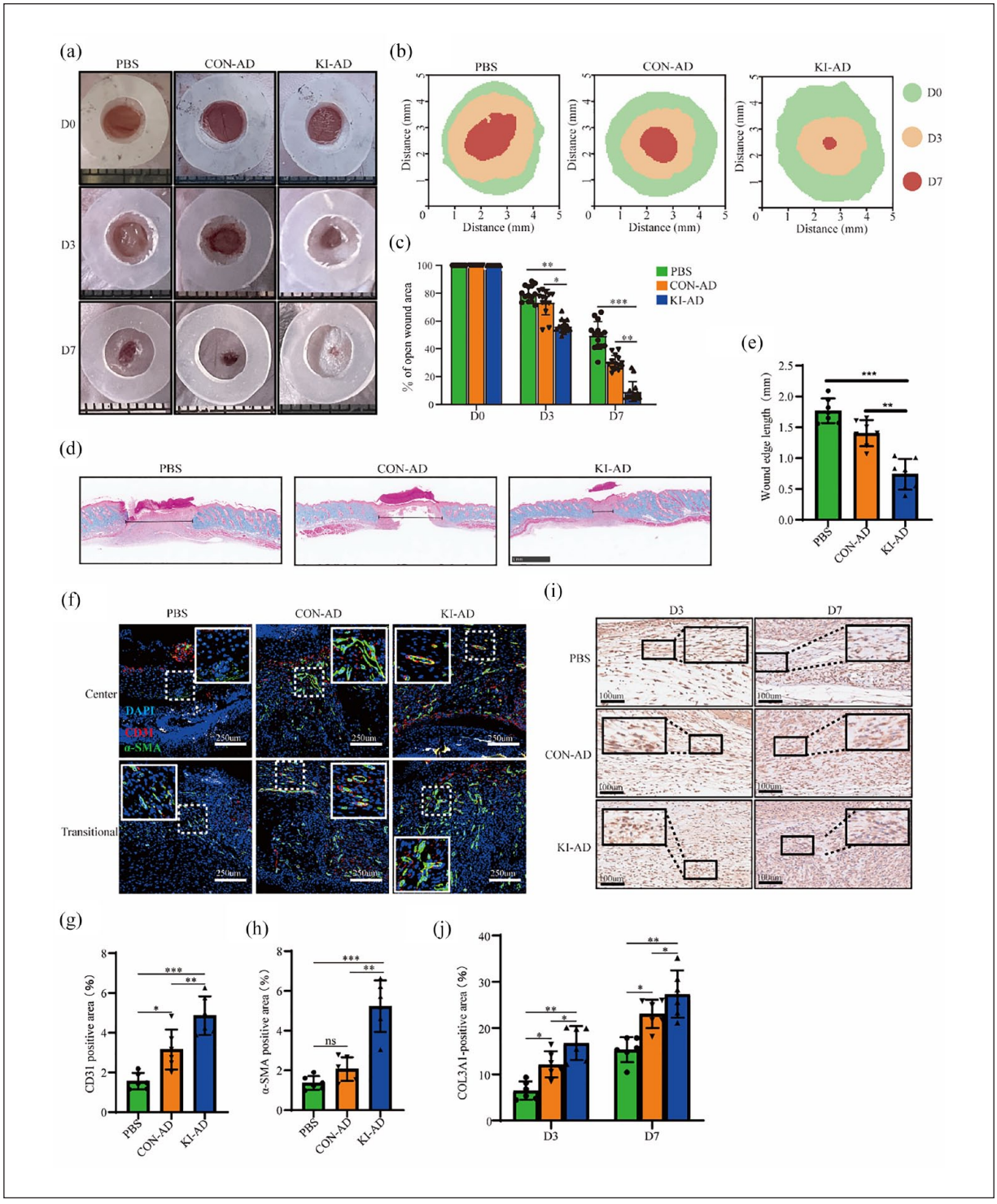

Figure 4. Tail vein infusion of *PSGL-1*-engineered ADSCs accelerated chronic wound healing. (a) Representative images of the healing process in wounds treated with PBS, CON-ADSCs, and KI-ADSCs ($n = 14$). (b) Traces of wound-bed closure for 7 days. (c) The rate of wound closure from day 0 to day 7 was quantified based on the digital images of wounds. (d and e) Representative H&E staining images of wounds and quantitative analysis on days 7 after surgery. Double-headed black arrows indicate the edges of nonhealing scars ($n = 6$). (f–h) Representative images and quantitative analysis of immunofluorescence staining for CD31 (red fluorescence signal) and α-SAM (green fluorescence signal) at the wound site 7 days after treatment ($n = 6$). Scale bars, 250 μm. (i and j) Representative images and quantitative analysis of COL3A1 immunohistochemical staining of wounds at 3 and 7 days after treatment ($n = 6$). Scale bars, 100 μm. Data are shown as mean ± SD. Independent-sample t-test (two-tailed) was used for statistical comparisons between two groups; One–way ANOVA followed by Tukey post hoc test was used for statistical comparisons between multiple groups.
*$p < 0.05$, **$p < 0.01$, ***$p < 0.001$.

indicated that the knock-in of *PSGL-1* enhanced the homing, retention, and viability of ADSCs at skin lesions.

KI-ADSCs promoted wound healing in mice

To investigate the potential therapeutic benefits associated with increased cell homing and retention, wound healing was evaluated in this study. The wounds were assessed at 0, 3, and 7 days post-injury. Throughout the healing process, the wound area gradually decreased over time. Notably, the KI-ADSCs treatment group exhibited significantly enhanced wound healing from days 3 to 7 compared to the PBS and CON-ADSCs treatment groups (Figure 4(a)–(c)). At the end of the observation period for wound healing kinetics, the newly formed skin tissues were collected for further histological analysis. On day 7, the KI-ADSCs treated group displayed a greater presence of granulation tissue, a shorter wound length, and a thicker dermal layer with well-formed epidermal cells in comparison to the PBS group and CON-ADSCs group (Figure 4(d) and (e)), indicating a higher degree of wound re-epithelialization following KI-ADSCs treatment (Supplemental Figure 9). To evaluate angiogenesis in the vicinity of the wounds, CD31 and α-SMA immunofluorescence staining were performed. The KI-ADSCs treated group exhibited a greater number of CD31 and α-SMA positive cells compared to the CON-ADSCs treatment group and PBS treatment group (Figure 4(f)–(h)), suggesting that KI-ADSCs infusion enhanced angiogenesis within the wounds. Furthermore, the deposition of extracellular matrix (ECM) around the wound was analyzed. IHC staining demonstrated higher expression of collagen III in the wounds of the KI-ADSCs treatment group on the 3rd and 7th-day post-injury (Figure 4(i) and (j)). In conclusion, the knock-in of *PSGL-1* promoted the engraftment and retention of ADSCs and facilitated the healing process of wounds through enhanced granulation tissue formation, re-epithelialization, and angiogenesis at the wound site.

PSGL-1 *knock-in and platelets binding on ADSCs increased ADSC proliferation, migration, anti-apoptosis, and paracrine*

We next sought to determine the mechanism responsible for the enhanced reparative effects of KI-ADSCs. Numerous studies have demonstrated that PRP can promote the proliferation, migration, maintenance of stemness, and immunomodulatory properties of MSCs.[37,38] Thus, this study aimed to assess the functional impact of gene knock-in and platelet binding on ADSCs. CCK-8 results revealed that *PSGL-1* knock-in significantly augmented cell proliferation compared to CON-ADSCs, with further enhancement observed upon platelet binding (Figure 5(a)). MSCs predominantly contribute to wound repair through cytokine secretion. Therefore, we examined the expression of specific cytokines associated with wound healing and angiogenesis using RT-qPCR and ELISA. In comparison to CON-ADSCs, the *b-FGF, ANG1, COL1a1, HGF, CXCL-12, COL3a1, IGF*, and *VEGFA* were significantly increased in KI-ADSCs. Platelet binding further amplified this effect (Figure 5(b)). Additionally, ELISA results demonstrated that the secretion levels of IGF, VEGFA, and HGF were significantly higher in KI-ADSCs conditioned media compared to CON-ADSCs conditioned media, with further enhancement observed upon platelet binding (Figure 5(c)). To evaluate migration and anti-apoptotic abilities, scratch assay and flow cytometry analysis were performed. The results indicated a slight superiority of KI-ADSCs over CON-ADSCs in terms of anti-apoptotic ability (Figure 5(d) and (e)) and migratory capability (Figure 5(f) and (g)); however, no statistically significant difference was observed. Notably, when KI-ADSCs were combined with platelets, both migration and anti-apoptotic abilities were significantly improved (Figure 5(e) and (g)). These results suggested that the knock-in of *PSGL-1* promoted the proliferation and paracrine of ADSCs, and the binding of platelets further improved the function of ADSCs. However, *PSGL-1* knock-in alone didn't further amplify ADSC migration and anti-apoptosis under our experimental conditions. Notably, when ADSCs were bound to platelets, we observed a significant improvement in their migration and anti-apoptosis ability.

Functional effects of conditioned media derived from ADSCs on HUVECs and human immortalized keratinocytes (HaCaTs)

In vivo study demonstrated that KI-ADSCs significantly promoted wound healing, increased angiogenesis, enhanced collagen deposition, and promoted re-epithelialization in mice. Determined to uncover the mechanisms prompting these effects, we proceeded with an in vitro study. Given the substantial alterations observed in cytokine release from KI-ADSCs, we postulated that the knock-in of *PSGL-1* perhaps plays a role in promoting wound healing by improving ADSCs' paracrine functions. To explore this further, we cultured HUVECs and HaCaTs in a conditioned media derived from ADSCs. CCK-8 analysis revealed that the conditioned media from KI-ADSCs (KI-CM) significantly stimulated HUVECs proliferation in comparison to the control group (CON-CM). Remarkably, proliferation was further potentiated in the KI+PRP group (KI+PRP-CM) (Figure 6(a)). In addition, similar results were observed in the scratch assay (Figure 6(b) and (c)) and tube formation assay (Figure 6(d)–(f)), in which the KI-CM partly promoted the functional exhibition of HUVECs compared with CON-CM, while the KI+PRP-CM group exhibited the best migration and tube formation among all groups. In vitro experiments with HaCaTs cells, we obtained similar results to those of HUVECs; both KI-CM and KI+PRP-CM notably promoted cell proliferation and migration compared to CON-CM (Supplemental Figure 10). Taken together, these

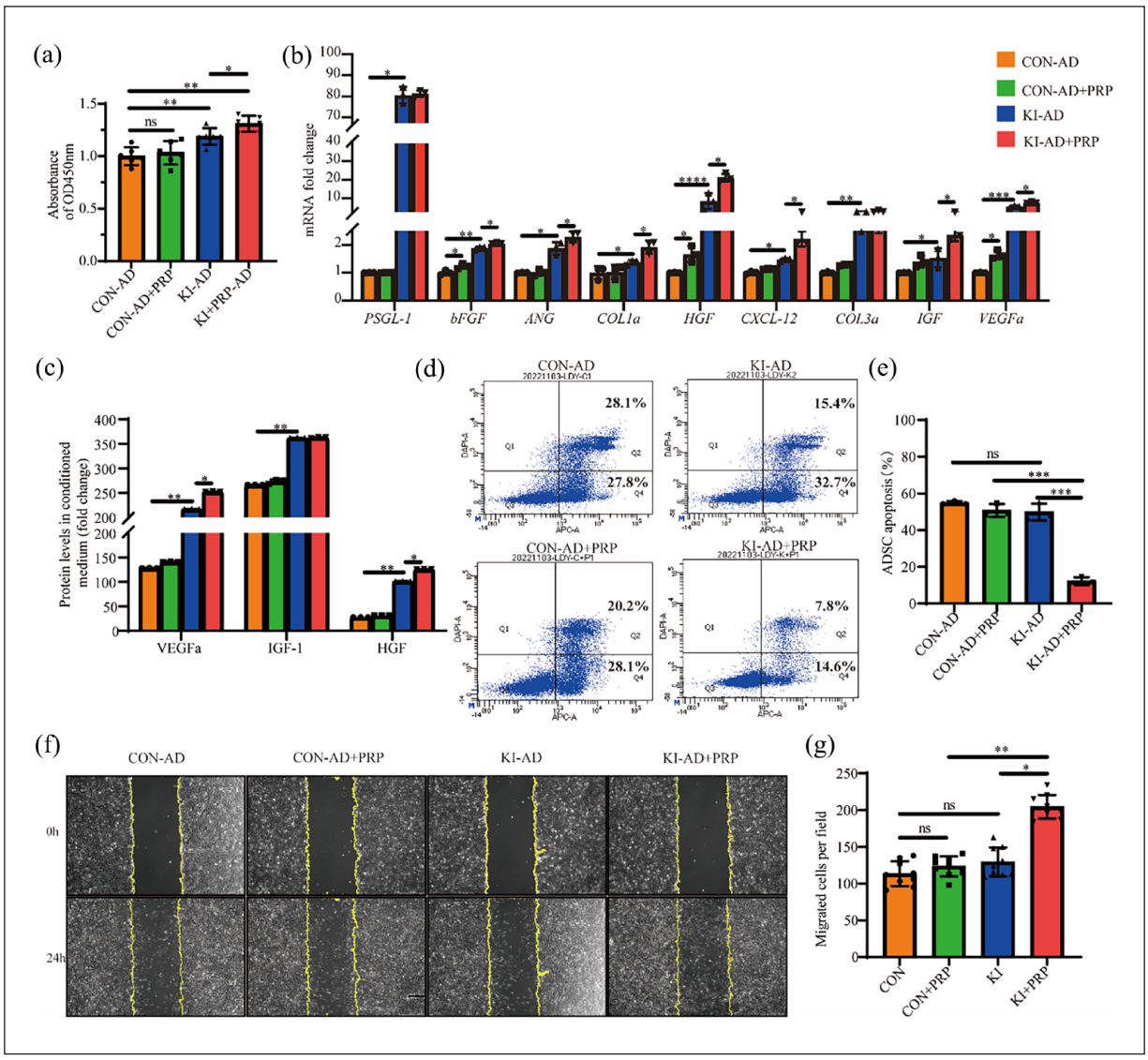

Figure 5. The knock-in of *PSGL-1* and platelet binding on ADSCs led to an increase in ADSC proliferation, migration, anti-apoptotic activity, and paracrine signaling. (a) Cell viability was determined by CCK-8 assay ($n = 6$). (b and c) RT-qPCR and ELISA analysis of the expression for genes of interest in CON-ADSCs and KI-ADSCs ($n = 3$). (d and e) Flow cytometry analysis of the apoptosis of CON-ADSCs and KI-ADSCs ($n = 3$). Flow cytometry analysis of the apoptosis of CON-ADSCs and KI-ADSCs (n=3). Flow cytometry was performed on cells treated with 250uM H_2O_2 for 12 hours. (f and g) Representative scratch test images of ADSCs incubated with different conditioned media at 0 and 12 h, and the rate of wound area closure after 12 h (%) ($n = 9$). Scale bars, 200 μm. Data are shown as mean ± SD. Independent-sample *t*-test (two-tailed) was used for statistical comparisons between two groups; One–way ANOVA followed by Tukey post hoc test was used for statistical comparisons between multiple groups. $^{*}p < 0.05$, $^{**}p < 0.01$, $^{***}p < 0.001$, $^{****}p < 0.0001$.

in vitro studies demonstrated that *PSGL-1* knock-in improves the ADSC secretome, thereby enhancing their ability to regulate angiogenesis and stimulate the proliferation and migration of HUVECs and HaCaTs.

Knock-in of PSGL-1 *activated* β*-catenin signaling*

PSGL-1 has been reported to function not only in the regulation of leukocyte and T-cell migration to inflammatory tissues,[39,40] but also as a transmembrane receptor for cellular signal transduction.[41,42] To further clarify the molecular mechanisms underpinning the observed effects of *PSGL-1* knock-in on ADSCs, we undertook an extensive molecular exploration. To this end, RNA sequencing analysis of KI-ADSCs and CON-ADSCs were performed to identify differentially expressed genes implicated in crucial biological processes. The results revealed 288 genes that were differentially expressed in KI-ADSCs compared to CON-ADSCs (197 upregulated and 91 downregulated). These genes were involved in important biological processes such as the Wnt signaling pathway,

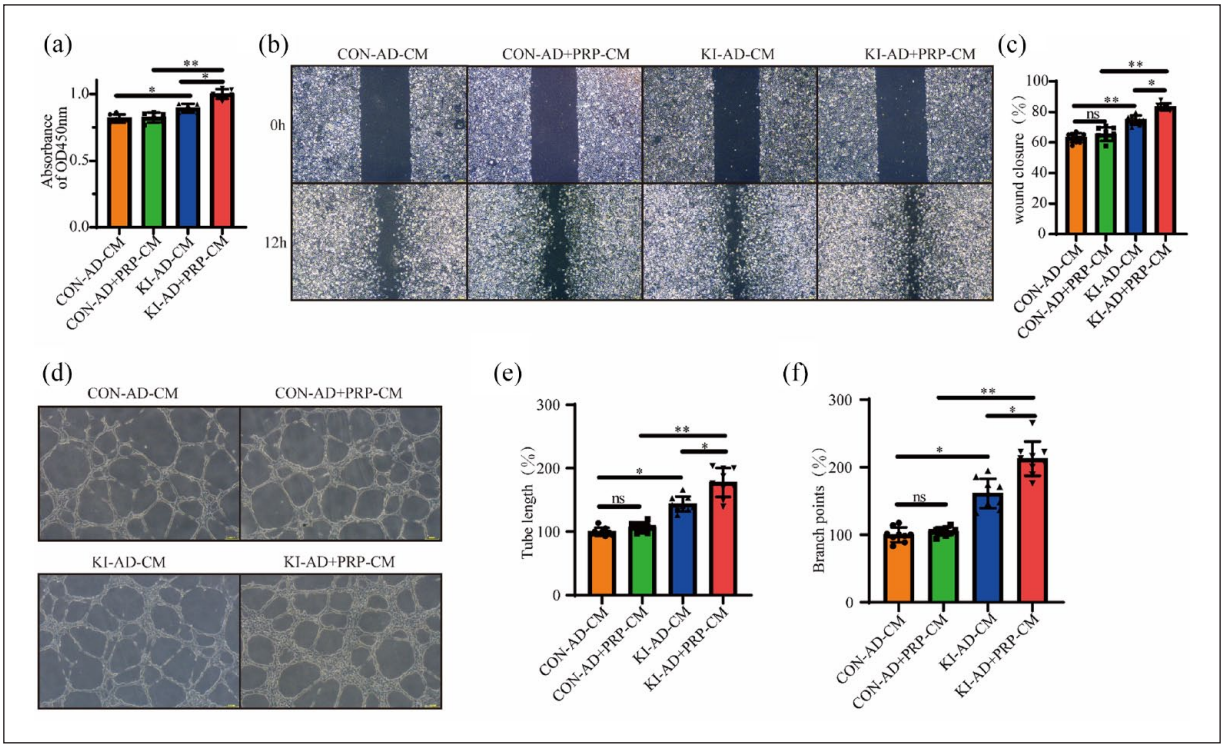

Figure 6. Different conditioned media on HUVECs function. (a) CCK-8 assay was used to assess the viability of HUVECs incubated with different conditioned media ($n = 6$). (b and c) Representative scratch test images of HUVECs incubated with different conditioned media at 0 and 12 h, and the rate of wound area closure after 12 h (%) ($n = 9$). Scale bars, 200 μm. (d–f) Representative tube formation images of HUVECs incubated with different conditioned media for 8 h, as well as quantitative analysis ($n = 9$). Scale bars, 200 μm. Data are shown as mean ± SD. Independent-sample *t*-test (two-tailed) was used for statistical comparisons between two groups; One–way ANOVA followed by Tukey post hoc test was used for statistical comparisons between multiple groups.
$^{*}p < 0.05$, $^{**}p < 0.01$.

angiogenesis, myeloid leukocyte migration, and endothelial cell proliferation (Figure 7(a)). The Wnt signaling pathway is one of the most important signaling pathways in embryonic and organ development, participating in the regulation of cell proliferation, differentiation, migration, and apoptosis.[43] We sought to explore the possibility of PSGL-1 affecting the ADSC function via modulating the Wnt/β-catenin signaling pathway. The Western blotting results showed that the expression of total and active β-catenin was significantly increased in the cytoplasm of KI-ADSCs compared with CON-ADSCs. Importantly, the increase in active β-catenin was also observed in the nucleus of KI-ADSCs, suggesting the potential role of PSGL-1 knock-in in promoting the translocation of active β-catenin to the nucleus and possibly triggering the Wnt/β-catenin signaling pathway in ADSCs, thus enhancing their functional performance (Figure 7(b)–(d)). Finally, we demonstrated by co-immunoprecipitation that *PSGL-1* knock-in promoted the formation of the PSGL-1/β-catenin complex in KI-ADSCs. Moreover, we showed that PSGL-1 can interact practically with active β-catenin (Figure 7(e)).

PSGL-1 *knock-in promoted ADSCs function in a* β*-catenin dependent manner*

Finally, to examine the causal relationship between the activation of WNT/β-catenin signaling and the altered phenotype of KI-ADSC. Short interfering RNA (siRNA) was used to knock down β-catenin (Figure 8(a) and (b)). CCK-8 results showed that the proliferation ability of KI-ADSCs was significantly decreased after siRNA treatment (Figure 8(c)). RT-qPCR and ELISA results revealed that inhibiting β-catenin led to a notable decrease in cytokine secretion (Figure 8(d) and (e)). Besides, conditioned media of ADSCs was collected after the inhibition of β-catenin to culture the HUVECs and HaCaTs. The results of CCK-8, cell scratch assay, and tube formation assay showed that the proliferation, migration, and pro-angiogenic effects of KI+Si-CM were significantly inhibited compared with those of KI-CM (Figure 8(f)–(k)) (Supplemental Figure 11). Taken together, *PSGL-1* knock-in modulated the functionality of HUVECs and HaCaTs cells by stimulating the paracrine action of ADSCs through Wnt/β-catenin signaling pathway activation (Figure 9).

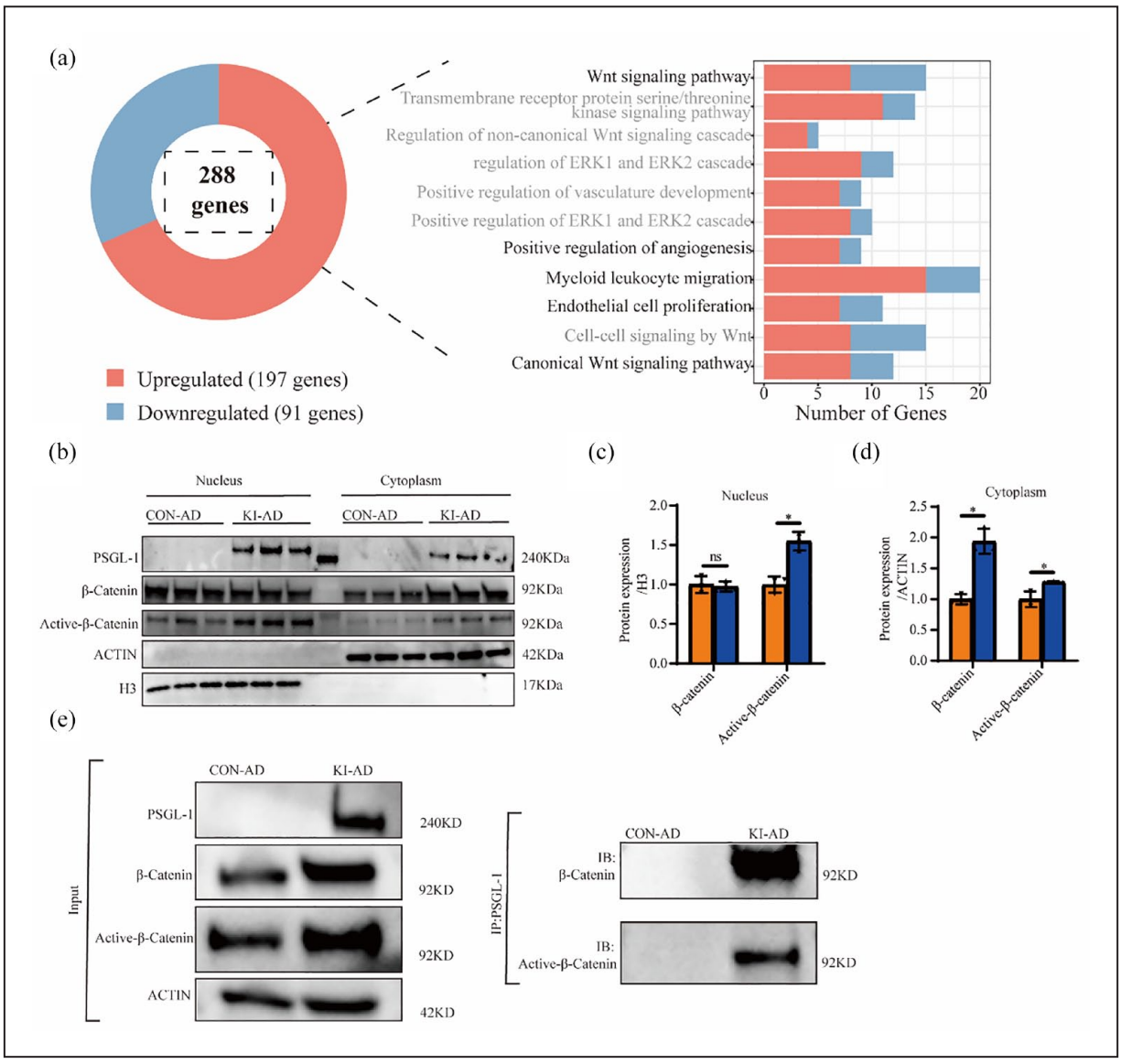

Figure 7. *PSGL-1* knock-in increased β-catenin expression and activation. (a) Pathway analysis of differentially expressed genes regulated in KI-ADSCs versus CON-ADSCs. (b–d) Western blot analysis of PSGL-1, β-catenin, and active-β-catenin levels in the nucleus and cytoplasm of CON-ADSCs and KI-ADSCs ($n = 3$). (e) Co-immunoprecipitation (Co-IP) analysis of PSGL-1 with β-catenin and active-β-catenin in ADSC whole-cell lysis. Data are shown as mean ± SD. Independent-sample *t*-test (two-tailed) was used for statistical comparisons between two groups.
*$p < 0.05$, **$p < 0.01$.

Discussion

The primary advantage of MSC therapy over other traditional therapeutic approaches is its ability to migrate actively to damaged tissues, also known as "homing." However, numerous studies have shown that regardless of the pathological models used, only a small fraction of intravenously transfused MSCs can reach the damaged tissues,[44,45] so one of the biggest challenges in the clinical application of MSCs is to improve their homing efficiency. Several approaches have been employed to enhance MSC homing, including targeted administration, magnetic guidance, genetic modification, cell surface engineering, in vitro priming, target tissue modification, and radiotherapy techniques. Despite the potential for modest enhancement in the homing of MSCs, it is important to acknowledge the inherent limitations associated with these approaches.[10] These approaches primarily target distinct stages of the MSC homing process, aiming to improve cell migration or adhesion. In this study, we employed the inherent capability of platelets to specifically home to the injured sites, as well as the prompt upregulation of Selectin family proteins following skin injury. By integrating PSGL-1 into ADSCs, this research achieved a considerable enhancement of homing efficiency in a skin wound model. Additionally, this approach has the notable benefit of concurrently

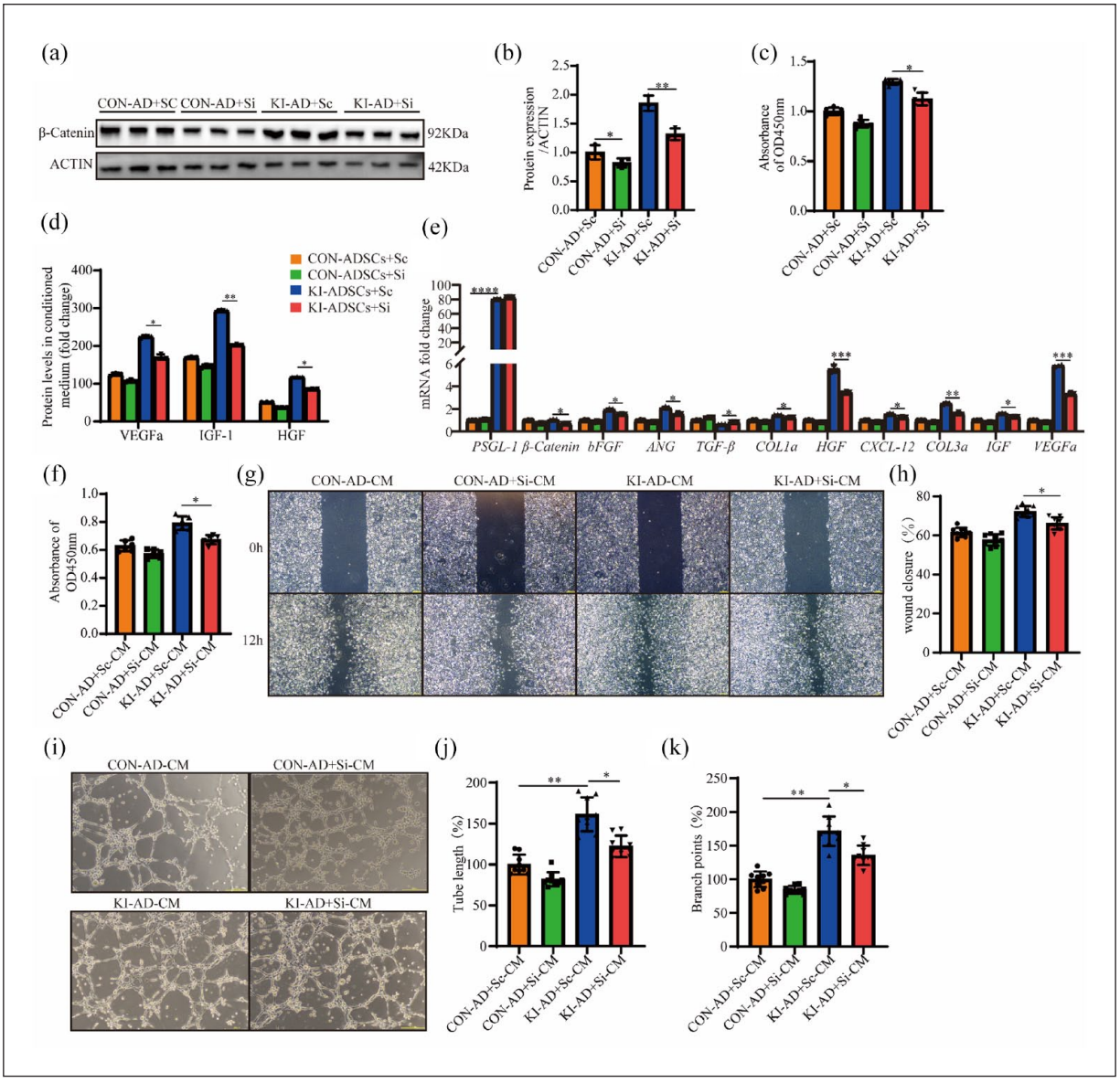

Figure 8. *PSGL-1* knock-in affected the paracrine of ADSCs in a β-catenin dependent manner. (a and b) Western blotting analysis of β-catenin levels in cells treated with β-catenin siRNA (Siβ-cat) or scramble RNA (Scβ-cat) for 48 h ($n = 3$). (c) CCK-8 assay was used to evaluate the cell viability of CON-ADSCs and KI-ADSCs after Siβ-cat or Scβ-cat pretreatment ($n = 6$). (d and e) ELISA and RT-qPCR analysis of the expression for genes of interest in CON-ADSC and KI-ADSC after Siβ-cat or Scβ-cat pretreatment ($n = 3$). (f) CCK-8 analysis of the viability of HUVECs incubated with different conditioned media ($n = 6$). (g and h) Representative scratch test images of HUVECs incubated with different conditioned media at 0 and 12 h, and the rate of wound area closure after 12 h (%) ($n = 9$). Scale bars, 200 μm. (i–k) Representative tube formation images of HUVECs incubated with different conditioned media for 8 h, as well as quantitative analysis ($n = 6$). Scale bars, 200 μm. Data are shown as mean ± SD. Independent-sample *t*-test (two-tailed) was used for statistical comparisons between two groups; One–way ANOVA followed by Tukey post hoc test was used for statistical comparisons between multiple groups.
*$p < 0.05$, **$p < 0.01$, ***$p < 0.001$, ****$p < 0.0001$.

enhancing the migration and adhesion of ADSCs to the injured site.

MSCs are typically infused in two ways: (1) systemic infusion (i.e., intravenously or intraarterial), and (2) through local tissue-specific delivery. Although local delivery may enhance cell retention, it has been reported as more invasive compared to the less invasive and easily reproducible intravenous route.[20,46] Furthermore, the decreased expression of related homing molecules (chemokine receptors, adhesion molecules, etc.) during cell culture and within the harsh pathological microenvironment results in a low survival rate and inefficient migration of transplanted cells to target organs.[7,44,47] Consequently, the ability of anchoring-dependent cells to adhere and homing to the injured site is limited.[48,49] In this study, our aimed was to enhance the homing efficiency of

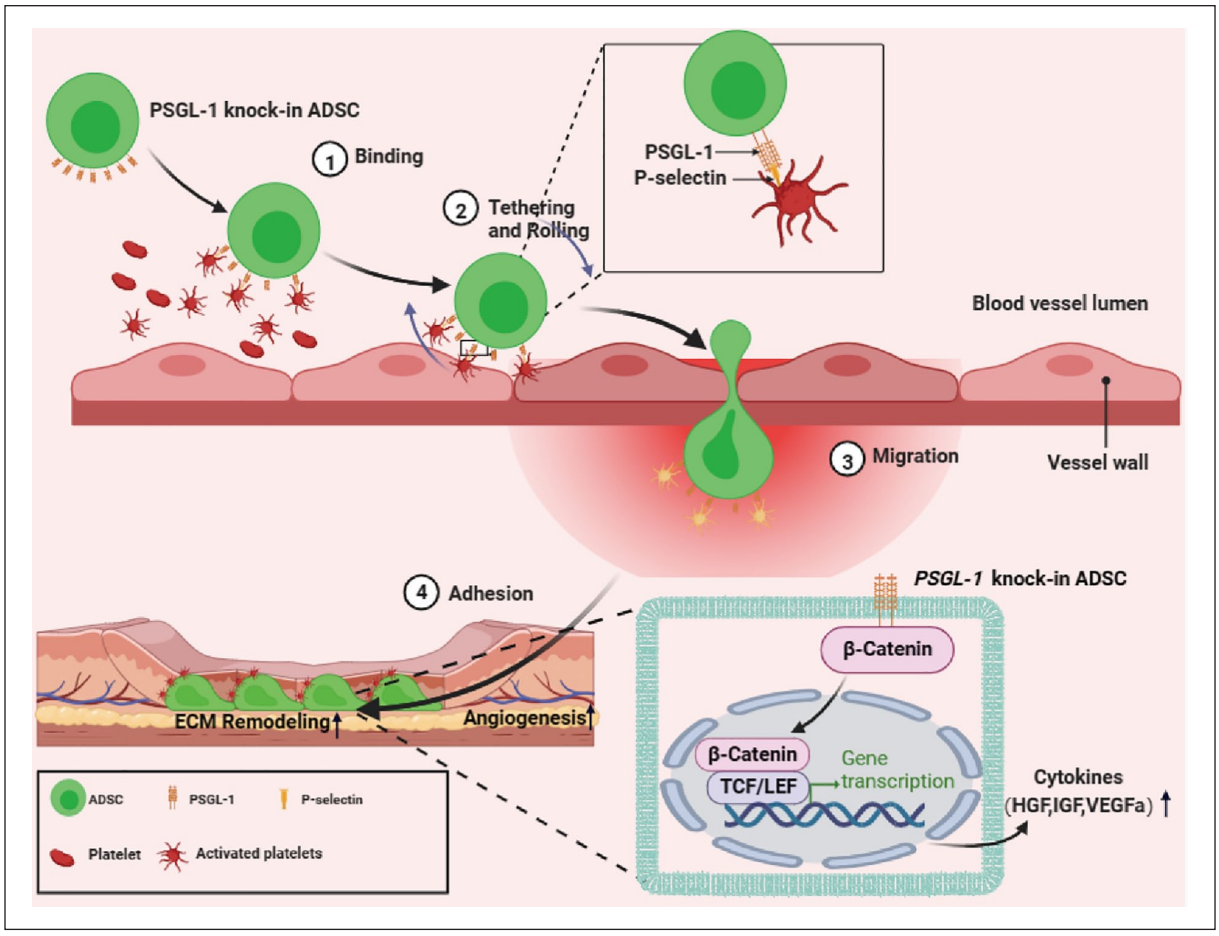

Figure 9. Summary diagram. Knock-in of *PSGL-1* via CRISPR/Cas9 was designed to simultaneously promote the migration and adhesion of ADSCs to the injury site. Due to the innate injury-finding ability of platelets which guide ADSCs to injured wounds for repair.

ADSCs by leveraging the natural homing characteristics of platelets. To achieve this, we employed CRISPR/Cas9 technology to enable ADSCs to express PSGL-1 through targeted knock-in, thereby facilitating their interaction with platelets. Previous research suggests that the initial tethering and rolling of platelet aggregates, which assist $CD34^+$ progenitor cells under flow conditions, is mediated by the interaction between P-selectin on the platelet's surface and PSGL-1 on $CD34^+$ progenitor cells.50 Similarly, in vitro co-culture experiments conducted by Daub et al. have shown that human platelets can recruit $CD34^+$ cells through specific adhesion receptors, namely P-selectin and β1 and β2 integrins.[51] Langer et al.[52] have demonstrated that adherent platelets play a crucial role in capturing mouse embryonic EPC (eEPC) at sites of vascular lesions under dynamic flow conditions. The depletion of platelets has been found to significantly reduce MSC homing to inflammatory sites.[53] Apart from platelets themselves, platelet-derived extracellular vesicles have been observed to bind to mouse stem cells and human $CD34^+$ cells through antigens such as P-selectin and integrin Mac-1 (CD11b-CD18), thus enhancing progenitor attachment to the vascular endothelium and resulting in increased cell homing and transplantation.[54] Liu et al.[55] have demonstrated that Platelet microparticles (PMPs) can transfer several homing and adhesion molecules, including CD41, P-selectin, CXCR4, PSGL-1, and CD11b, into cells. Hence, platelets play a critical role in the homing and engraftment of stem cells through direct contact or spatial proximity. This is attributed to platelets serving as a significant source of extracellular adhesion molecules/chemokine receptors, growth factors, and cytokines that are necessary for the homing process. Previous studies have shown that intravenously infused MSCs are mainly "trapped" in the lungs. The results of a clinical study showed that the "action path" of stem cells after intravenous transfusion is a gradual "dynamic" process. Intravenously transfused MSCs accumulate first in the lungs, and after 2 h, they are captured in the liver and spleen.[28] So, considering that the lungs are reported as a 'reservoir' for platelets,[56] it is plausible that the binding of ADSCs to platelets could accelerate their migration out of the lungs. In this study, we found that 1 day after cell transplantation, most of the cells were distributed in the liver. Meanwhile the binding of ADSCs to platelets significantly reduced their non-targeted distribution in the liver.

Besides their involvement in the homing and engraftment of stem cells, platelets exert a discernible influence on the functional performance of these cells. Research conducted by Peng et al.[57] revealed that bone marrow-derived mesenchymal stem cells (BM-MSCs) can be reprogrammed to withstand harsh microenvironments through pretreatment with platelet clots. Additionally, this pretreatment can enhance the regenerative potential of the stem cells by increasing the release of soluble factors through the PDGF-α-PI3K-AkT-Nf-κb pathway. Levoux et al.[58] demonstrated that platelets can transfer respiratory-competent mitochondria to MSCs primarily via dynamin-dependent clathrin-mediated endocytosis. This process has been shown to enhance the therapeutic efficacy of MSC transplantation in various mouse models of tissue injury. This is due to the paracrine action of various growth factors from platelets, such as platelet-derived growth factor (PDGF), VEGF, and IGF. The concentration ratios of these growth factors closely resemble those found in the natural environment of the body. In our study, we found that the binding of platelets to ADSCs could not only promote cell proliferation, migration, and release of some cytokines but also enhance the resistance of ADSCs to harsh pathological microenvironments, thereby improving the therapeutic effect of ADSCs. Significantly, the presence of platelets adhered to stem cells can influence the inherent functionality of these cells, without necessitating high concentrations of PRP in co-culture.

Beyond these, we also conducted experiments in mechanism exploration. Our data suggested that the knock-in of *PSLG-1* activated the canonical WNT signaling by increasing the expression of active β-catenin. This activation subsequently induced the secretion of cytokines, leading to an expedited process of wound healing. β-*catenin* gene silencing significantly blocked the release of cytokines induced by *PSGL-1* knock-in and abolished the promotion of KI-ADSCs conditioned medium on the function of HUVECs and HaCaTs. These results suggested that β-*catenin* is pivotal in *PSGL-1* knock-in–induced gene expression and subsequent functional regulation. According to reports, PSGL-1 is known to interact with the actin cytoskeleton and act as an adaptor to facilitate intracellular signaling.[42] The binding of selectins to PSGL-1 activates Src family kinases.[59] Furthermore, the signaling triggered by the antibody ligation of PSGL-1 on neutrophils leads to the phosphorylation of various proteins, including ERK1 and ERK2, indicating that PSGL-1 has the ability to regulate crucial cellular functions.[60] In support of this concept, the activation of mTOR has also been reported to occur downstream of PSGL-1 signaling in macrophages; and this activation leads to the expression of Rho-associated kinase-1 (ROCK-1), indicating a potential signaling pathway involving phosphoinositide 3 kinase (PI3K).[61] Similarly, it has been demonstrated that the ligation of PSGL-1 by the antibody on Jurkat T cells induces clustering of β1 integrin, which is reliant on PI3K activation.[62] Moreover, the ligation of PSGL-1 induces the secretion of cytokines by macrophages, dendritic cells (DCs), and T cells, suggesting a positive role in immune regulation.[63–66]

Ultimately, our study did not observe any immunogenic alterations in the mice administered with ADSCs. This outcome could potentially be attributed to the utilization of a serum-free culture system. Notably, a recent investigation has identified bovine apolipoprotein B-100 as the primary immunogen in therapeutic cells cultured with FBS67. Additionally, other research studies have examined the compromised immunosuppressive capacity of MSCs cultivated in media supplemented with FBS or human serum.[68-71]

In summary, our study has shed light on the cell therapy field with the following novelties. First, we developed a methodology, which possesses the potential to be employed in the management of diverse afflictions. This is primarily due to the indispensable role of platelets in the process of inflammation. Secondly, we successfully achieved simultaneous site-directed integration of large fragments with about 4.3 kb sequences and multiple genes into primary cells. Due to the constraints imposed by the synthesis techniques of single-stranded oligodeoxynucleotide (ssODN) and double-stranded DNA (dsDNA), the nonviral approach is confined to an insertion size of approximately 1.5 kb. Third, instead of manipulating the cell membranes through in vitro modification techniques such as membrane fusion or modification, we employed autologous platelets to tackle the issue of MSCs homing. This strategy circumvents the potential loss of numerous surface receptors present on the platelet membrane, which may have side effects on the interaction between MSCs and platelets. Fourth, *PSGL-1* knock-in simultaneously promoted migration and adhesion to the injured site of MSCs.

There are also some limitations in this study. First, the overall efficiency of gene knock-in is suboptimal, making it unsuitable for large-scale clinical production. Secondly, the mechanisms of how platelets affect stem cell function have not been clearly understood. Thirdly, platelets possess tumor-targeting properties, yet the role of stem cells in cancer therapy remains a subject of controversy. Fourth, it is noted that our evaluation of the risks associated with platelet aggregation and thrombosis has thus far been preliminary. A comprehensive safety assessment is imperative to provide a more detailed understanding of these potential risks. Interestingly, the amounts of MSC-platelet aggregates in the blood of MI patients were significantly higher than that of healthy controls, which contributed to better prognosis.[72] Furthermore, before clinical application, additional toxicity studies employing higher doses, such as 5 or even 10 times the therapeutic dosage, are imperative.

Conclusion

The low homing efficiency of MSCs is a significant obstacle to their clinical application. Specifically, cell homing refers to the ability of transplanted cells to migrate and adhere to damaged tissues. To address this issue, genetic engineering has been used to modify MSCs. This study integrated *PSGL-1* into the genome of ADSCs using a Cas9-AAV6-based genome editing platform. The results demonstrated that *PSGL-1* knock-in enhances the binding of ADSCs to platelets and their adhesion to injured sites. Furthermore, the administration of KI-ADSCs significantly improved the homing efficiency and residence at the site of skin lesions in mice. Mechanistically, *PSGL-1* knock-in promoted the release of therapeutic cytokines by activating the canonical WNT/β-catenin signaling, accelerating the healing of wounds through the promotion of angiogenesis, re-epithelialization, and granulation tissue formation at the wound site. This study provided an innovative strategy for simultaneously addressing the challenges of poor migration and adhesion of MSCs.

Acknowledgements

We gratefully acknowledge for the technical assistance of Core Facility of West China Hospital (Li Chai, Yi Li and Xing Xu).

Author's contribution

B-MZ and D-YL designed the study. D-YL, Y-ML, and TD conducted in vitro cell experiments and analyzed the collected data. Y-ML, D-YL, LY, TD, XZ, Q-YP, and XZ. conducted in vivo animal experiments, Y-ML and D-YL analyzed the collected data. D-YL and B-MZ wrote the manuscript. All authors have read and agreed to the published version of the manuscript.

Data availability

The manuscript contains all the necessary data to support the stated conclusions. If there is a need for additional relevant data, interested individuals may obtain them from the authors by making a reasonable request.

Declaration of conflicting interests

The author(s) declared no potential conflicts of interest with respect to the research, authorship, and/or publication of this article.

Funding

The author(s) disclosed receipt of the following financial support for the research, authorship, and/or publication of this article: This study was supported by the National Natural Science Foundation of China (82274647), the Natural Science Foundation of Sichuan Province (2023YFH0013), the UTHSC/WCHSU CORNET Award (YB2019003), the Special Fund for CRISPR/Cas9 Gene Editing Technology of the Regenerative Medicine Research Center of West China Hospital (161170012), and study on the protective effect and mechanism of exercise on myocardial ischemia(21H1303)

Ethics approval and consent to participate

The project titled "Enhanced interaction between genome-edited mesenchymal stem cells and platelets improves wound healing in mice" was submitted for ethics approval on March 18, 2022, and was conducted in compliance with the guidelines presented in the Declaration of Helsinki. The research obtained approval from the Biomedical Ethics Review Committee of West China Hospital of Sichuan University (No. 20220318012). Additionally, we took all necessary measures to minimize any discomfort or distress that the animals may have experienced during the research.

Consent for publication

Not applicable.

ORCID iD

Bing-Mei Zhu https://orcid.org/0000-0001-5369-1931

Supplemental material

Supplemental material for this article is available online.

References

1. Swann G. The skin is the body's largest organ. *J Vis Commun Med* 2010; 33(4): 148–149.
2. Nethi SK, Das S, Patra CR, et al. Recent advances in inorganic nanomaterials for wound-healing applications. *Biomater Sci* 2019; 7(7): 2652–2674.
3. Sorg H, Tilkorn DJ, Hager S, et al. Skin wound healing: an update on the current knowledge and concepts. *Eur Surg Res* 2017; 58(1–2): 81–94.
4. Xue M and Jackson CJ. Extracellular matrix reorganization during wound healing and its impact on abnormal scarring. *Adv Wound Care (New Rochelle)* 2015; 4(3): 119–136.
5. Rezaie F, Momeni-Moghaddam M and Naderi-Meshkin H. Regeneration and repair of skin wounds: various strategies for treatment. *Int J Low Extrem Wounds* 2019; 18(3): 247–261.
6. Sen CK. Human wound and its burden: updated 2020 compendium of estimates. *Adv Wound Care (New Rochelle)* 2021; 10(5): 281–292.
7. Dekoninck S and Blanpain C. Stem cell dynamics, migration and plasticity during wound healing. *Nat Cell Biol* 2019; 21(1): 18–24.
8. Nourian Dehkordi A, Mirahmadi Babaheydari F, Chehelgerdi M, et al. Skin tissue engineering: wound healing based on stem-cell-based therapeutic strategies. *Stem Cell Res Ther* 2019; 10(1): 111.
9. Caplan AI. Why are MSCs therapeutic? New data: new insight. *J Pathol* 2009; 217(2): 318–324.
10. Ullah M, Liu DD and Thakor AS. Mesenchymal stromal cell homing: mechanisms and strategies for improvement. *iScience* 2019; 15: 421–438.
11. Nitzsche F, Muller C, Lukomska B, et al. Concise review: MSC adhesion cascade-insights into homing and transendothelial migration. *Stem Cells* 2017; 35(6): 1446–1460.
12. Zhang X, Huang W, Chen X, et al. CXCR5-overexpressing mesenchymal stromal cells exhibit enhanced homing and

can decrease contact hypersensitivity. *Mol Ther* 2017; 25(6): 1434–1447.
13. Huang Y, Wang J, Cai J, et al. Targeted homing of CCR2-overexpressing mesenchymal stromal cells to ischemic brain enhances post-stroke recovery partially through PRDX4-mediated blood-brain barrier preservation. *Theranostics* 2018; 8(21): 5929–5944.
14. Dhoke NR, Kaushik K and Das A. Cxcr6-based mesenchymal stem cell gene therapy potentiates skin regeneration in murine diabetic wounds. *Mol Ther* 2020; 28(5): 1314–1326.
15. Shen Z, Wang J, Huang Q, et al. Genetic modification to induce CXCR2 overexpression in mesenchymal stem cells enhances treatment benefits in radiation-induced oral mucositis. *Cell Death Dis* 2018; 9(2): 229.
16. Golebiewska EM and Poole AW. Platelet secretion: from haemostasis to wound healing and beyond. *Blood Rev* 2015; 29(3): 153–162.
17. Mu D, Zhang XL, Xie J, et al. Intracoronary transplantation of mesenchymal stem cells with overexpressed integrin-linked kinase improves cardiac function in porcine myocardial infarction. *Sci Rep* 2016; 6: 19155.
18. Quiroz HJ, Valencia SF, Shao H, et al. E-selectin-overexpressing mesenchymal stem cell therapy confers improved reperfusion, repair, and regeneration in a murine critical limb ischemia model. Front Cardiovasc Med 2021; 8: 826687.
19. Cho YH, Cha MJ, Song BW, et al. Enhancement of MSC adhesion and therapeutic efficiency in ischemic heart using lentivirus delivery with periostin. *Biomaterials* 2012; 33(5): 1376–1385.
20. Misra V, Ritchie MM, Stone LL, et al. Stem cell therapy in ischemic stroke: role of IV and intra-arterial therapy. *Neurology* 2012; 79(13 Suppl 1): S207–S212.
21. Saboor M, Ayub Q, Ilyas S, et al. Platelet receptors; an instrumental of platelet physiology. *Pak J Med Sci* 2013; 29(3): 891–896.
22. Wilkinson HN and Hardman MJ. Wound healing: cellular mechanisms and pathological outcomes. *Open Biol* 2020; 10(9): 200223.
23. Li Z, Hu S and Cheng K. Platelets and their biomimetics for regenerative medicine and cancer therapies. *J Mater Chem B* 2018; 6(45): 7354–7365.
24. Chen L, Zhou Z, Hu C, et al. Platelet membrane-coated nanocarriers targeting plaques to deliver anti-CD47 antibody for atherosclerotic therapy. *Research (Wash D C)* 2022; 2022: 9845459.
25. Shinde A, Illath K, Gupta P, et al. A review of single-cell adhesion force kinetics and applications. *Cells* 2021; 10(3): 577.
26. Mousa SA. Cell adhesion molecules: potential therapeutic and diagnostic implications. *Mol Biotechnol* 2008; 38(1): 33–40.
27. Etzioni A. Adhesion molecules—their role in health and disease. *Pediatr Res* 1996; 39(2): 191–198.
28. Gholamrezanezhad A, Mirpour S, Bagheri M, et al. In vivo tracking of 111In-oxine labeled mesenchymal stem cells following infusion in patients with advanced cirrhosis. *Nucl Med Biol* 2011; 38(7): 961–967.
29. Zaongo SD, Liu Y, Harypursat V, et al. P-selectin glycoprotein ligand 1: a potential HIV-1 therapeutic target. *Front Immunol* 2021; 12: 710121.
30. Ruster B, Gottig S, Ludwig RJ, et al. Mesenchymal stem cells display coordinated rolling and adhesion behavior on endothelial cells. *Blood* 2006; 108(12): 3938–3944.
31. Yang WH, Nussbaum C, Grewal PK, et al. Coordinated roles of ST3Gal-VI and ST3Gal-IV sialyltransferases in the synthesis of selectin ligands. *Blood* 2012; 120(5): 1015–1026.
32. Bak RO and Porteus MH. CRISPR-mediated integration of large gene cassettes using AAV donor vectors. *Cell Rep* 2017; 20(3): 750–756.
33. Martin RM, Ikeda K, Cromer MK, et al. Highly efficient and marker-free genome editing of human pluripotent stem cells by CRISPR-Cas9 RNP and AAV6 donor-mediated homologous recombination. *Cell Stem Cell* 2019; 24(5): 821–828 e5.
34. Fu YW, Dai XY, Wang WT, et al. Zhang, dynamics and competition of CRISPR-Cas9 ribonucleoproteins and AAV donor-mediated NHEJ, MMEJ and HDR editing. *Nucleic Acids Res* 2021; 49(2): 969–985.
35. Wilkinson AC, Dever DP, Baik R, et al. Cas9-AAV6 gene correction of beta-globin in autologous HSCs improves sickle cell disease erythropoiesis in mice. *Nat Commun* 2021; 12(1): 686.
36. Dominici M, Le Blanc K, Mueller I, et al. Minimal criteria for defining multipotent mesenchymal stromal cells. The international society for cellular therapy position statement. *Cytotherapy* 2006; 8(4): 315–317.
37. Kawase T. Platelet-rich plasma and its derivatives as promising bioactive materials for regenerative medicine: basic principles and concepts underlying recent advances. *Odontology* 2015; 103(2): 126–135.
38. Astori G, Amati E, Bambi F, et al. Platelet lysate as a substitute for animal serum for the ex-vivo expansion of mesenchymal stem/stromal cells: present and future. *Stem Cell Res Ther* 2016; 7(1): 93.
39. Haddad W, Cooper CJ, Zhang Z, et al. P-selectin and P-selectin glycoprotein ligand 1 are major determinants for Th1 cell recruitment to nonlymphoid effector sites in the intestinal lamina propria. *J Exp Med* 2003; 198(3): 369–377.
40. Martin-Fontecha A, Baumjohann D, Guarda G, et al. CD40L+ CD4+ memory T cells migrate in a CD62P-dependent fashion into reactive lymph nodes and license dendritic cells for T cell priming. *J Exp Med* 2008; 205(11): 2561–2574.
41. Sanchez-Madrid F and Serrador JM. Bringing up the rear: defining the roles of the uropod. *Nat Rev Mol Cell Biol* 2009; 10(5): 353–359.
42. Alonso-Lebrero JL, Serrador JM, Dominguez-Jimenez C, et al. Polarization and interaction of adhesion molecules P-selectin glycoprotein ligand 1 and intercellular adhesion molecule 3 with moesin and ezrin in myeloid cells, *Blood* 2000; 95(7): 2413–2419.
43. Nusse R and Clevers H. Wnt/beta-catenin signaling, disease, and emerging therapeutic modalities. *Cell* 2017; 169(6): 985–999.
44. De Becker A and Riet IV. Homing and migration of mesenchymal stromal cells: how to improve the efficacy of cell therapy? *World J Stem Cells* 2016; 8(3): 73–87.
45. Chavakis E, Urbich C and Dimmeler S. Homing and engraftment of progenitor cells: a prerequisite for cell therapy. *J Mol Cell Cardiol* 2008; 45(4): 514–522.

46. Kang ES, Ha KY and Kim YH. Fate of transplanted bone marrow derived mesenchymal stem cells following spinal cord injury in rats by transplantation routes. *J Korean Med Sci* 2012; 27(6): 586–593.
47. SenGupta S, Parent CA and Bear JE. The principles of directed cell migration. *Nat Rev Mol Cell Biol* 2021; 22(8): 529–547.
48. Sart S, Ma T and Li Y. Preconditioning stem cells for in vivo delivery. *Biores Open Access* 2014; 3(4): 137–149.
49. Vilquin JT, Catelain C and Vauchez K. Cell therapy for muscular dystrophies: advances and challenges. *Curr Opin Organ Transplant* 2011; 16(6): 640–649.
50. de Boer HC, Verseyden C, Ulfman LH, et al. Fibrin and activated platelets cooperatively guide stem cells to a vascular injury and promote differentiation towards an endothelial cell phenotype. *Arterioscler Thromb Vasc Biol* 2006; 26(7): 1653–1659.
51. Stellos K, Seizer P, Bigalke B, et al. Platelet aggregates-induced human CD34+ progenitor cell proliferation and differentiation to macrophages and foam cells is mediated by stromal cell derived factor 1 in vitro. *Semin Thromb Hemost* 2010; 36(2): 139–145.
52. Langer H, May AE, Daub K, et al. Adherent platelets recruit and induce differentiation of murine embryonic endothelial progenitor cells to mature endothelial cells in vitro. *Circ Res* 2006; 98(2): e2–10.
53. Teo GS, Yang Z, Carman CV, et al. Intravital imaging of mesenchymal stem cell trafficking and association with platelets and neutrophils. *Stem Cells* 2015; 33(1): 265–277.
54. Janowska-Wieczorek A, Majka M, Kijowski J, et al. Platelet-derived microparticles bind to hematopoietic stem/progenitor cells and enhance their engraftment. *Blood* 2001; 98(10): 3143–3149.
55. Liu B, Liao C, Chen J, et al. Significance of increasing adhesion of cord blood hematopoietic cells and a new method: platelet microparticles. *Am J Hematol* 2003; 74(3): 216–217.
56. Lefrancais E, Ortiz-Munoz G, Caudrillier A, et al. The lung is a site of platelet biogenesis and a reservoir for haematopoietic progenitors. *Nature* 2017; 544(7648): 105–109.
57. Peng Y, Huang S, Wu Y, et al. Platelet rich plasma clot releasate preconditioning induced PI3K/AKT/NFkappaB signaling enhances survival and regenerative function of rat bone marrow mesenchymal stem cells in hostile microenvironments. *Stem Cells Dev* 2013; 22(24): 3236–3251.
58. Levoux J, Prola A, Lafuste P, et al. Platelets facilitate the wound-healing capability of mesenchymal stem cells by mitochondrial transfer and metabolic reprogramming. *Cell Metab* 2021; 33(2): 283–299.e9.
59. Xu T, Zhang L, Geng ZH, et al. P-selectin cross-links PSGL-1 and enhances neutrophil adhesion to fibrinogen and ICAM-1 in a Src kinase-dependent, but GPCR-independent mechanism. *Cell Adh Migr* 2007; 1(3): 115–123.
60. Hidari KI, Weyrich AS, Zimmerman GA, et al. Engagement of P-selectin glycoprotein ligand-1 enhances tyrosine phosphorylation and activates mitogen-activated protein kinases in human neutrophils. *J Biol Chem* 1997; 272(45): 28750–28756.
61. Fox R, Nhan TQ, Law GL, et al. PSGL-1 and mTOR regulate translation of ROCK-1 and physiological functions of macrophages. *EMBO J* 2007; 26(2): 505–515.
62. Luo J, Li C, Xu T, et al. PI3K is involved in beta1 integrin clustering by PSGL-1 and promotes beta1 integrin-mediated Jurkat cell adhesion to fibronectin. *Mol Cell Biochem* 2014; 385(1–2): 287–295.
63. Urzainqui A, Martinez del Hoyo G, Lamana A, et al. Functional role of P-selectin glycoprotein ligand 1/P-selectin interaction in the generation of tolerogenic dendritic cells. *J Immunol* 2007; 179(11): 7457–7465.
64. Ba XQ, Chen CX, Xu T, et al. Engagement of PSGL-1 upregulates CSF-1 transcription via a mechanism that may involve Syk. *Cell Immunol* 2005; 237(1): 1–6.
65. Damle NK, Klussman K, Dietsch MT, et al. GMP-140 (P-selectin/CD62) binds to chronically stimulated but not resting CD4+ T lymphocytes and regulates their production of proinflammatory cytokines. *Eur J Immunol* 1992; 22(7); 1789–1793.
66. Celi A, Pellegrini G, Lorenzet R, et al. P-selectin induces the expression of tissue factor on monocytes. *Proc Natl Acad Sci U S A* 1994; 91(19): 8767–8771.
67. Sakamoto N, Tsuji K, Muul LM, et al. Bovine apolipoprotein B-100 is a dominant immunogen in therapeutic cell populations cultured in fetal calf serum in mice and humans. *Blood* 2007; 110(2) 501–508.
68. Kocaoemer A, Kern S, Kluter H, et al. Human AB serum and thrombin-activated platelet-rich plasma are suitable alternatives to fetal calf serum for the expansion of mesenchymal stem cells from adipose tissue. *Stem Cells* 2007; 25(5): 1270–1278.
69. Lee JY, Kang MH, Jang JE, et al. Comparative analysis of mesenchymal stem cells cultivated in serum free media. *Sci Rep* 2022; 12(1): 8620.
70. Poloni A, Maurizi G, Serrani F, et al, Human AB serum for generation of mesenchymal stem cells from human chorionic villi: comparison with other source and other media including platelet lysate. *Cell Prolif* 2012; 45(1): 66–75.
71. Shih DT and Burnouf T. Preparation, quality criteria, and properties of human blood platelet lysate supplements for ex vivo stem cell expansion. *N Biotechnol* 2015; 32(1): 199–211.
72. Song YL, Jiang H, Jiang NG, et al. Mesenchymal stem cell-platelet aggregates increased in the peripheral blood of patients with acute myocardial infarction and might depend on the stromal cell-derived factor 1/CXCR4 axis, *Stem Cells Dev* 2019; 28(24): 1607–1619.